Optical chaos and oscillations in photorefractive $LiNbO_3$:Fe

Obukhovsky V. and Lemeshko V.

Taras Shevchenko National University of Kyiv, 64 Volodymyrska Street,
Kyiv 01033, Ukraine e-mail: obukhovsky@univ.kiev.ua

Received: 16.12.2013

Abstract. Autowaves of scattering appear under excitation of nonlinear $LiNbO_3$: Fe crystals by a focused laser radiation, manifesting themselves as moving light-ring structures. A periodic behaviour of generation of the rings could be related to competition of refractive index gratings of the two types, reflecting and transmission ones. A chaotic regime arises if the control parameters, the pump intensity and the impurity concentration, become less than a threshold.

Keywords: $LiNbO_3$: Fe crystals, photorefraction, optical chaos, autowave light scattering

PACS: 42.65.Hw, 42.65.Sf
UDC: 535.321+544.032.65+530.182.2

1. Introduction and experimental data

A phenomenon of autowave light scattering (AWLS) has been experimentally revealed in the study [1]. Later on, the effect has been investigated in Refs. [2, 3]. The AWLS appears as a backward scattering with a conical indicatrix in the experiments with steady-state illumination of $LiNbO_3$: Fe crystals by a focused laser beam propagating along the direction opposite to the optic axis z (i.e., along $-z$ – see Fig. 1). Contrary to some other kinds of photorefractive light scattering, the effect is considerably non-stationary. The AWLS intensity (quasi-)periodically oscillates in time during photoexcitation of a crystal by a steady-state laser radiation, and the temporal modulation depth can approach 100%. While the oscillations evolve, the spatial distribution of the scattering intensity changes in the following sequence: (a) the scattering appears near the surface of a cone with a fixed initial angle $\theta_0 \neq 0$, (b) the cone widens, and (c) the scattering radiation disappears. Then the process repeats (quasi-)periodically.

We begin with a brief report on our experimental data on the above effect, develop a relevant theory and, finally, give a critical comparison of the theory and the experimental results. A He-Cd laser (the radiation wavelength $\lambda = 0.44$ μm and the power $P_L = 20$ mW) has been used in our experiments. The radiation is focused by a lens with the focal length $F = 10$ cm into the region close to the front surface of a z-cut of $LiNbO_3$: Fe crystal. The thickness of the crystal is $\ell = 0.3$ cm and the impurity concentration $n_d = 0.03$ weight %. The AWLS is observed on the screen (see Fig. 1a) as bright rings forming the scattering cones, with the initial angle θ_0 being equal to 1.5^o and the angle at which the scattering disappears amounting to $\theta_{dis} \approx 3.5^o$ (Fig. 1b). The cone angle widens with increasing concentration n_d so that the values $\theta_0 \approx 3.5^o$ and $\theta_{dis} \approx 8^o$ are reached at

n_d = 0.07 weight %. The radiation power concentrated inside the scattering rings is as high as ~ 80% of the pump power. The oscillation period (1÷10 s in our experiments) depends on the pump parameters, such as the power and the conditions of focusing. Notice that intentional increase in the intensity of light reflected from the output surface of the sample by a supplementary mirror causes increasing oscillation intensity.

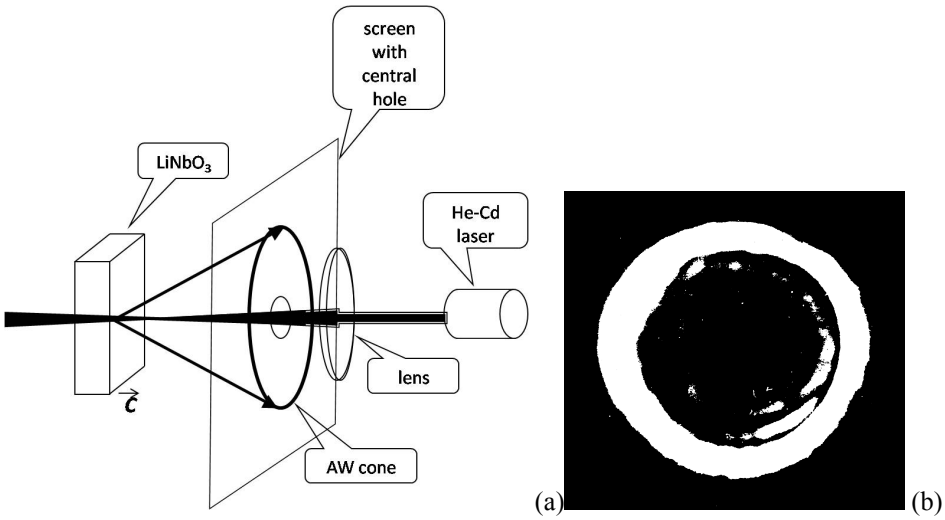

Fig. 1. Scheme of our experiments on exciting the AWLS (a) and a picture of the scattering ring (b).

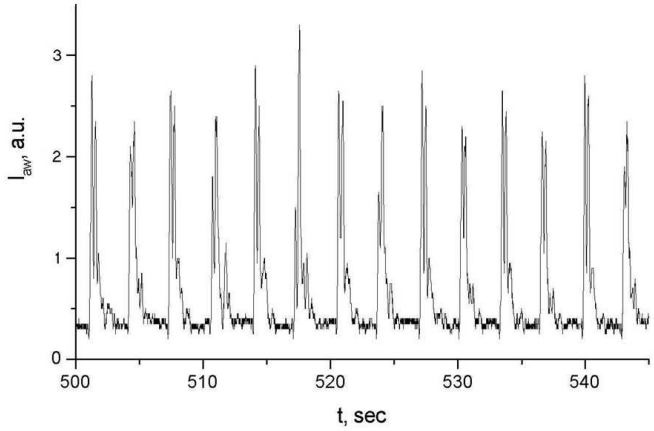

Fig. 2. Temporal dependence of the AWLS signal.

An example of temporal dependences of the AWLS is shown in Fig. 2. The scattering light intensity has been measured by a photodetector (photodiode) placed into the scattering ring. The AWLS is not observed when the crystal is excited along the +z direction. The shape of AWLS indicatrix follows that of the exciting beam. The indicatrix represents a conical surface only when a cylindrical laser-pump beam is focused by a spherical lens. In the case of cultriform pumping, the scattering indicatrix represents two parallel planes moving away from each other.

It should be noted that the regime of AWLS could only be implemented when the pump intensity exceeds some threshold value, $I_L >> I_L^0$. In our experiments the threshold intensity is

$I_L^0 \approx 40$ W/cm^2 at $\lambda = 0.44$ μm. For I_L lower than the threshold I_L^0, a chaotic regime is detected, i.e. a set of chaotically flickering spots of irregular shapes is observed. The threshold intensity value depends on the pump wavelength λ_L and increases when λ_L shifts towards the 'red' spectral region.

A periodic appearance of the scattering rings could be associated with competition of the longitudinal and transverse charge-transfer mechanisms in photorefractive crystals. The latter results in dynamic instability of a reflecting grating, which is lost provided that a transmission grating with sufficiently large amplitudes appears.

2. Theory of AWLS

A concept of running waves of impurity-centre overcharge [4] may be used to explain the AWLS effect. The instabilities can appear in a nonlinear system 'photorefractive crystal + laser radiation'. In their turn, these can lead to formation of different transverse structures [5-8]. Spatial-temporal instabilities in the systems of this kind have been considered in Refs. [9, 10]. The theory presented below is based on these results.

Let us consider a nonlinear photorefractive crystal with no inversion centre. The crystal is illuminated by a stationary laser beam corresponding to a TEM_{00} mode. We use the following geometry for our calculations: the central wave vector of the pump beam is directed along the *z* axis (the latter can be parallel or antiparallel to the optic axis *z* of the crystal) and the pump polarization $\mathbf{e}_1$ lies in the plane *xy*, the origin being placed at the pump-beam centre on the front side of crystal (see Fig. 1). The symmetry group of the crystal is 3m. The crystal is taken to be infinite in the transverse directions (i.e., in the *xy* plane) and to have the thickness ℓ.

The laser field inside the crystal will be presented as follows:

$$\mathbf{E}^{\omega} = \mathbf{A}_1(\mathbf{r},t)\exp\left[i\left(k_0 z - \omega\ t\right)\right] + \mathbf{A}_{-1}(\mathbf{r},t)\exp\left[-i\left(k_0 z + \omega\ t\right)\right] + c.c., \tag{1}$$

with $k_0 = \omega\sqrt{\varepsilon_0}\,/c$. The amplitudes $\mathbf{A}_{\pm 1}$ are considered to be smooth functions that depend on the coordinates and time. Using the technique [10], we separate a part $\mathbf{E}_s^f(\mathbf{r})$ slowly varying along *z* and an oscillating dynamic part in the structure of internal electric field $\mathbf{E}^f$ in the crystal:

$$\mathbf{E}^f = \mathbf{E}_s^f(\mathbf{r},t) + \mathbf{U}^f(\mathbf{r},\ t)\exp\left[2ik_0 z\right] + c.c. \tag{2}$$

The amplitudes $\mathbf{E}_s^f(\mathbf{r},t)$ and $\mathbf{U}^f(\mathbf{r},\ t)$ are also taken to be smooth functions that depend on the coordinates and time. The second summand in Eq. (2) corresponds to taking reflective holograms into account.

The terms corresponding to electrooptic change of the refractive index $\Delta\hat{\varepsilon}_{EO} = \hat{\chi}\mathbf{E}^f$ (with $\hat{\chi}$ being the electrooptic tensor) and the dielectric permittivity fluctuations $\delta\hat{\varepsilon}(\vec{r})$ (e.g., those originated from crystal growth) can be separated in the dielectric permittivity $\hat{\varepsilon} = \hat{\varepsilon}_0 + \Delta\hat{\varepsilon}_{EO}(\mathbf{r},t) + \delta\hat{\varepsilon}(\mathbf{r})$ at the excitation frequency ω. The electrooptic modulation may be described as follows: $\Delta\hat{\varepsilon}_{EO}(\mathbf{r},t) = \Delta\hat{\varepsilon}_0(\mathbf{r},t) + \Delta\hat{\varepsilon}_2(\mathbf{r},t)\exp[2ik_0 z] + c.c.$ Here we distinguish the part $\Delta\hat{\varepsilon}_2 = \hat{\chi}\mathbf{U}^f$ linked with formation of the system of reflective holographic gratings (with the wave vector $2k_0$) and the part $\Delta\hat{\varepsilon}_0 = \hat{\chi}\mathbf{E}_S^f$ imposed by spatial charge redistribution on the scales $\Delta l_S >> 1/k_0$. By analogy, the seeds of different types of gratings

$\delta\hat{\varepsilon}(\mathbf{r}) = \delta\hat{\varepsilon}_R(\mathbf{r}) + \delta\hat{\varepsilon}_2(\mathbf{r})\exp[2ik_0 z] + c.c.$ can also be separated in the expansion $\delta\hat{\varepsilon}(\mathbf{r})$. The other scattering components will be neglected. In our notation, the reduced equations for the amplitudes of the direct (A_1) and backward (A_{-1}) waves take the form [4]

$$\begin{cases} \dfrac{\partial \mathbf{A}_1}{\partial z} - \left(\dfrac{i}{2k_0}\right)\Delta_\perp \mathbf{A}_1 = i\dfrac{k_0}{2\varepsilon_0}\left[\Delta\hat{\varepsilon}_0 \mathbf{A}_1 + \left(\Delta\hat{\varepsilon}_2 + \delta\hat{\varepsilon}_2(\vec{\mathbf{r}})\right)\mathbf{A}_{-1}\right], \\ \dfrac{\partial \mathbf{A}_{-1}}{\partial z} + \left(\dfrac{i}{2k_0}\right)\Delta_\perp \mathbf{A}_{-1} = -i\dfrac{k_0}{2\varepsilon_0}\left[\hat{\Delta}\varepsilon_0 \mathbf{A}_{-1} + \left(\Delta\hat{\varepsilon}_2^* + \delta\hat{\varepsilon}_2^*(\mathbf{r})\right)\mathbf{A}_1\right]. \end{cases} \tag{3}$$

Notice that the absorption of the optical waves is neglected in what follows.

In accordance with the experimental data [1, 3], assume that $\mathbf{A}_{\pm 1} = \mathbf{e}_1 A_{\pm 1}(\mathbf{r}, t)$ so that the polarization of the light waves retains during scattering. Then the scalar functions can be introduced:

$$\Delta\varepsilon_2 = \mathbf{e}_1\left(\hat{\chi}\mathbf{U}^f\right)\mathbf{e}_1,\ \delta\varepsilon = \mathbf{e}_1\delta\hat{\varepsilon}_2\mathbf{e}_1,\ \Delta\varepsilon_0 = \mathbf{e}_1\left(\hat{\chi}\mathbf{E}_s^f\right)\mathbf{e}_1. \tag{4}$$

The amplitude $\Delta\varepsilon_2$ of dielectric-permittivity modulation imposed by the linear electrooptic effect can be divided into two parts:

$$\Delta\varepsilon_2 = \Delta\varepsilon_{\|} + \Delta\varepsilon_{\perp},\ \begin{cases} \Delta\varepsilon_{\|} = e_{1\,i} e_{1\,j} \chi_{i\,j,z} U_z^f \\ \Delta\varepsilon_{\perp} = e_{1\,i} e_{1j} \chi_{i\,j,\perp} U_{\perp}^f \end{cases}, \tag{5}$$

which is consistent with consideration of influence of both the longitudinal (U_z^f) and transverse ($U_\perp^f$) components of the internal field.

The internal electric field $\mathbf{E}^f$ may be found from the system of equations [11–13]:

$$\mathrm{div}\left(\hat{\varepsilon}^f \mathbf{E}^f\right) = 4\pi e\left(n_d^+ - n_e - n_a\right), \tag{6}$$

$$\mathrm{div}\left[e\hat{\mu} n_e \mathbf{E}^f + eD_0 \nabla n_e + \frac{\hat{\varepsilon}^f}{4\pi}\frac{\partial \mathbf{E}^f}{\partial t}\right] = -\mathrm{div}\left[I\left(n_d - n_d^+\right)\hat{\beta} : \mathbf{e}_1\mathbf{e}_1^*\right], \tag{7}$$

$$\frac{\partial n_d^+}{\partial t} = -\gamma_R n_e n_d^+ + \gamma_p I\left(n_d - n_d^+\right) + \gamma_T\left(n_d - n_d^+\right). \tag{8}$$

Here ε^f denotes the low-frequency dielectric permittivity, n_e the free-electron concentration, n_d, n_d^+ and n_a are concentrations of donors, ionized donors (traps) and acceptors, respectively, γ_R, γ_p and γ_T the coefficients of electron capture by the trap, photoionization and thermalization, respectively, $I = |A_1|^2 + |A_{-1}|^2 + A_1 A_{-1}^* \exp[2ik_0 z] + c.c.$ means the laser radiation intensity, e the absolute value of electron charge, μ the mobility, D_0 the diffusion coefficient, and $\hat{\beta}$ the photovoltaic tensor.

Further on, the acceptor levels are assumed to be located deeply enough and fully filled, and the donor traps to be filled fast enough (when compared to the period of autowave formation process). Similarly to Eq. (2), spatial-temporal distributions of the concentrations may be represented as follows:

$$
\begin{aligned}
n_e &= n_e^s(\mathbf{r},t) + \tilde{n}_e(\mathbf{r},t)\exp\left[2ik_0 z\right] + c.c.,\\
n_d^+ &= n_{ds}^+(\mathbf{r},t) + \tilde{n}_d^+(\mathbf{r},t)\exp\left[2ik_0 z\right] + c.c.,\\
n_d &= n_d^0 + \delta n_d(\mathbf{r})\exp\left[2ik_0 z\right] + c.c.,
\end{aligned}
\tag{9}
$$

i.e. the spatial harmonics ~ $2k_0$ are extracted from the spectra of concentration variations. The distribution functions of statistic fluctuations of the donor centre concentration $\delta n_d(\mathbf{r})$ will be considered as small ($|\delta n_d| << n_d^0$). We will take into consideration that the statistic dielectric permittivity $\hat{\varepsilon}^f$ and the conductivity $\hat{\sigma}$ are described by the tensors with nonzero diagonal components: $\varepsilon_{xx}^f = \varepsilon_{yy}^f = \varepsilon_\perp^f$, $\varepsilon_{zz}^f \neq \varepsilon_\perp^f$, $\varepsilon_{zz}^f \equiv \varepsilon_z^f$, and $\sigma_{xx} = \sigma_{yy} = \sigma_\perp^f$, $\sigma_{zz} \neq \sigma_\perp$.

Using the explicit form of convolution of the photovoltaic and electrooptic tensors given by Eqs. (5), with the pump polarization $\mathbf{e}_1 = \left(e_{ix},\ e_{iy}\right)$ for the crystals of the symmetry 3m, we have derived the equations for $\Delta\varepsilon_\parallel$ and $\Delta\varepsilon_\perp$, issuing from the vector equation for the internal field components (see Ref. [10]). As a consequence, we have arrived at the general system of equations, which describes the interaction of light waves with the photorefractive medium and involves the longitudinal and transverse components of the internal electric field:

$$
\begin{aligned}
&\frac{\partial}{\partial z}A_1 - ip_0\Delta_\perp A_1 = i\left(W_\parallel + W_\perp + \delta W\right)A_{-1},\\
&\frac{\partial}{\partial z}A_{-1}^* - ip_0\Delta_\perp A_{-1}^* = i\left(W_\parallel + W_\perp + \delta W\right)A_1^*,
\end{aligned}
\tag{10}
$$

$$
\begin{aligned}
&\tau_\perp\frac{\partial}{\partial t}W_\perp + W_\perp = -Q_\perp A_1 A_{-1}^* + iM_\perp W_\parallel - R_\perp^n(\mathbf{r}),\\
&\tau_\parallel\frac{\partial}{\partial t}W_\parallel + W_\parallel\left(1 - iM_\parallel\right) = -\left(Q_\parallel + iD\right)A_1 A_{-1}^* - R_\parallel^n(\mathbf{r}),
\end{aligned}
\tag{11}
$$

where $p_0 = 1/2k_0$. The main system of Eqs. (10) and (11) must be supplemented by the initial and boundary conditions:

$$A_1\left(z=0,x,y,t\right) = A_0\left(x,y\right),\ A_{-1}\left(z=\ell,x,y,t\right) = 0, \tag{12}$$

$$W_\parallel\left(\mathbf{r},\ t=0\right) = W_\perp\left(\mathbf{r},t=0\right) = 0. \tag{13}$$

The following notation is used in Eqs. (10) and (11):

$$W_\parallel(\mathbf{r},t) = \frac{k_0}{2}\Delta\varepsilon_\parallel(\mathbf{r},t),\ W_\perp(\mathbf{r},t) = \frac{k_0}{2}\Delta\varepsilon_\perp(\mathbf{r},t),\ \delta W(\mathbf{r}) = \frac{k_0}{2}\delta\varepsilon(\mathbf{r}). \tag{14}$$

It is worthwhile that the relaxation times $\tau_\parallel = \varepsilon_z^f / 4\pi\sigma_{zz}^f$ and $\tau_\perp = \varepsilon_\perp^f / 4\pi\sigma_\perp$ (i) depend on the pump intensity and (ii) can differ considerably from each other because of photoconductive anisotropy.

The following coupling parameters [10] are used in the system of Eqs. (11):

$$Q_\perp = \frac{\beta_{22}\chi_{22}}{\sigma_\perp^f}B_0,\ Q_\parallel = \frac{\beta_{31}\chi_{13}}{\sigma_{zz}^f}B_0,\ D = \frac{2\chi_{13}eD_0}{\sigma_{zz}^f(2\gamma_R n_{ds}^+ + \gamma_T)}, \tag{15}$$

$$M_\perp = \frac{\beta_{22}\chi_{22}}{\sigma_\perp\chi_{13}}B_1,\ M_\parallel = \frac{\beta_{31}}{\sigma_{zz}^f}B_1. \tag{16}$$

Here the notation

$$B_0 = \frac{k_0}{2}\left(n_d^0 - n_{ds}^+\right)\left(\frac{2\gamma_R n_{ds}^+ + \gamma_T}{2\gamma_R n_{ds}^+ + \gamma_p I_s + \gamma_T}\right),\ B_1 = \frac{k_0 e_z^f}{2\pi\ \ e}\left(\frac{\gamma_R n_{ds}^+ I_s}{2\gamma_R n_{ds}^+ + \gamma_p I_s + \gamma_T}\right).$$

is introduced. The volume (stationary) inhomogeneities of the impurity distribution induce a spatial modulation of the internal fields and the refractive index of the medium. They serve as Rayleigh (seed) scattering sources distributed over the sample volume. The influence of these inhomogeneities on the scattering processes is described by the summands $R_\perp^n(\mathbf{r})$ and $R_\parallel^n(\mathbf{r})$ appearing in Eq. (20). Their values are defined by the fluctuations of spatial distribution of the impurity centres (see Ref. [10]).

In what follows, the scattering intensity is considered small as compared to the pump-wave intensity, i.e. we have $|A_{-1}| << |A_1|$. In a zero-order approximation, the field $A_1(\mathbf{r})$ satisfies the homogeneous equation

$$\frac{\partial A_1}{\partial z} - ip_0 \Delta_\perp A_1 = 0\,. \tag{17}$$

If pumping is implemented by a focused Gaussian beam, the solution of Eq. (17) inside the beam-waist region acquires the form [14]

$$A_1(x, y, z \ge 0) \approx \sqrt{I_0}\,\exp\left[-\eta z - \frac{x^2 + y^2}{2\ \ \rho_0^2}\right], \tag{18}$$

where ρ_0 is the Gaussian beam radius. Here the origin of coordinates is placed into the pump-beam centre on the front side of the crystal ($z = 0$).

To solve the problem, we use Fourier transform over the transverse coordinates $\{x, y\}$ and Laplace transform over the longitudinal coordinate $\tilde{z} = \ell - z$. The system of Eqs. (11) linearized for the images $\tilde{W}_{\parallel,\perp}(\mathbf{q}, s, t)$ under the condition $|A_{-1}| << |A_1|$ becomes as follows:

$$\begin{cases} \tau_\parallel \dfrac{\partial \tilde{W}_\parallel}{\partial t} + \left(1 - iM_\parallel\right)\ \tilde{W}_\parallel = -i\left(Q_\parallel + iD\right) I_0 \psi_z \left(\tilde{W}_\parallel + \tilde{W}_\perp\right) - iI_0 \tilde{R}_\parallel(\mathbf{q}, s) \\ \tau_\perp \dfrac{\partial \tilde{W}_\perp}{\partial t} + \tilde{W}_\perp = -iQ_\perp \left(\tilde{W}_\parallel + \tilde{W}_\perp\right) I_0 \psi_z + iM_\perp \tilde{W}_\parallel - iI_0 \tilde{R}_\perp(\mathbf{q}, s) \end{cases}, \tag{19a}$$

$$\tilde{W}_\parallel(\mathbf{q}, s, t = 0) = 0,\ \tilde{W}_\perp(\mathbf{q}, s, t = 0) = 0\,, \tag{19b}$$

where the notation

$$\tilde{R}_{\parallel,\perp}(\mathbf{q}, s) = -i\,\tilde{R}_{\parallel,\perp}^n(\mathbf{q}, s) \big/ I_0 + \left(Q_{\parallel,\perp} + iD_{\parallel,\perp}\right)\psi_z(q, s)\delta\tilde{W}(\mathbf{q}, s), \tag{20a}$$

$$\psi_z(q, s) = i(q^2 / 2k_0) - s,\ (D_\parallel = D,\ D_\perp = 0) \tag{20b}$$

is used. Solving the system of inhomogeneous linear differential Eqs. (19), one obtains

$$\begin{aligned} \tilde{W}_\parallel(\mathbf{q}, s, t) &= I_0\left[R_1 + \frac{R_1\alpha_2 - R_2}{\alpha_1 - \alpha_2}\exp\left[\lambda_1 t\right] + \frac{R_2 - \alpha_1 R_1}{\alpha_1 - \alpha_2}\exp\left[\lambda_2 t\right]\right], \\ \tilde{W}_\perp(\mathbf{q}, s, t) &= I_0\left[R_2 + \alpha_1\frac{R_1\alpha_2 - R_2}{\alpha_1 - \alpha_2}\exp\left[\lambda_1 t\right] + \alpha_2\frac{R_2 - \alpha_1 R_1}{\alpha_1 - \alpha_2}\exp\left[\lambda_2 t\right]\right], \end{aligned} \tag{21}$$

with

$$\alpha_m(q,s) = i\frac{M_\perp - Q_\perp I_0\psi_z}{1+iQ_\perp I_0\psi_z + \tau_\perp\lambda_m},\ (m=1,\ 2)\,, \tag{22a}$$

$$R_1(\mathbf{q},s) = \frac{i\left[\tilde{R}_\perp\left(iQ_\parallel - D\right)I_0\psi_z - \tilde{R}_\parallel\left(1+iQ_\perp I_0\psi_z\right)\right]}{\left(1-iM_\parallel+\left(iQ_\parallel-D\right)I_0\psi_z\right)\left(1+iQ_\perp I_0\psi_z\right)-i\left(Q_\perp I_0\psi_z - M_\perp\right)\left(iQ_\parallel - D\right)},$$

$$R_2(\mathbf{q},s) = \frac{i\left[i\tilde{R}_\parallel\left(Q_\perp I_0\psi_z - M_\perp\right)-\tilde{R}_\perp\left(1-iM_\parallel+\left(iQ_\parallel-D\right)I_0\psi_z\right)\right]}{\left(1-iM_\parallel+\left(iQ_\parallel-D\right)I_0\psi_z\right)\left(1+iQ_\perp I_0\psi_z\right)-i\left(Q_\perp I_0\psi_z - M_\perp\right)\left(iQ_\parallel - D\right)}. \tag{22b}$$

The parameters $\lambda_m(q,s)$ are the roots of the master equation

$$\det\widehat{H}(q,s,\lambda) = 0\,, \tag{23}$$

where

$$\widehat{H}(q,s,\lambda) = \begin{pmatrix} \tau_\parallel\lambda + 1 - iM_\parallel + \left(iQ_\parallel - D\right)I_0\psi_z & \left(iQ_\parallel - D\right)I_0\psi_z \\ iQ_\perp I_0\psi_z - iM_\perp & \tau_\perp\lambda + 1 + iQ_\perp I_0\psi_z \end{pmatrix}. \tag{24}$$

3. Conditions for the appearance of AWLS

The roots of the master equation may be found by solving Eqs. (23) and (24):

$$\lambda_{1,2}(q,s) = -\frac{h_1(q,s)}{2} \pm \sqrt{\frac{h_1^2(q,s)}{4} - h_2(q,s)}\,, \tag{25}$$

where

$$h_1(q,s) = \frac{1-iM_\parallel + I_0\psi_z\left(iQ_\parallel - D\right)}{\tau_\parallel} + \frac{1+IQ_\perp I_0\psi_z}{\tau_\perp},$$

$$h_2(q,s) = \frac{\left(1-iM_\parallel+\left(iQ_\parallel-D\right)\ I_0\psi_z\right)\left(1+iQ_\perp I_0\psi_z\right)}{\tau_\parallel\tau_\perp} + \frac{i\left(Q_\perp I_0\psi_z - M_\perp\right)\left(iQ_\parallel - D\right)}{\tau_\parallel\tau_\perp}. \tag{26}$$

The absolute instability threshold of the system of Eqs. (19) corresponds to the condition $\mathrm{Re}\left(\lambda_1(q,s)\right) = \mathrm{Re}\left(\lambda_2(q,s)\right) = 0$. This can be reached when

$$\mathrm{Re}\left(h_1(q,s)\right) = 0,\ \mathrm{Im}\left(h_2(q,s)\right) = 0,\ \mathrm{Re}\left(h_2(q,s)\right) + \frac{\mathrm{Im}^2\left(h_1(q,s)\right)}{4} > 0\,. \tag{27}$$

In this case, a Hopf bifurcation appears in the system. Besides, the roots $\lambda_{1,2} = i\Omega_{1,2}$ are purely imaginary and so autooscillations with the frequencies $\Omega_{1,2}$ appear:

$$\Omega_{1,2} = -\frac{\mathrm{Im}\left(h_1\right)}{2} \pm \left[\mathrm{Re}\left(h_2\right) + \frac{\mathrm{Im}^2\left(h_1\right)}{4}\right]^{1/2}. \tag{28}$$

The conditions given by Eq. (27) may be transformed into a system of two linear equations with respect to $\mathrm{Re}\psi_z(\mathbf{q},s)$ and $\mathrm{Im}\psi_z(\mathbf{q},s)$. Using Eq. (20b), one can find the values $s = s_0$ and $q = q_0$ satisfying Eq. (27).

The estimations performed above demonstrate that the relations

$$\tau_\parallel << \tau_\perp,\ |D| << |Q_\parallel|,\ |Q_\perp| << |Q_\parallel| \tag{29}$$

hold true for the $LiNbO_3$:Fe crystals. Besides, it follows from Eqs. (27) and (28) that the AWLS regime is characterized by the following parameters:

(a) the autooscillation frequency [1]

$$\Omega_1 \approx \frac{1}{\tau_{||}} \frac{|DQ_\perp|}{Q_{||}^2}; \tag{30}$$

(b) the magnitude of transverse part of the wave vector of dynamic holographic grating $|\vec{q}_\perp| = q_0$, with

$$q_0 \approx \sqrt{-2k_0 I_0 Q_{||}}, \ (Q_{||} < 0); \tag{31}$$

(c) the coefficient of spatial gain

$$s_0 \approx -I_0 D, \ (D < 0). \tag{32}$$

It is obvious that the frequency depends linearly on the pump ($\Omega \sim I_0$) in the region of sufficiently high intensities, since $1/\tau_{||} \sim \sigma_{||} \sim n_e^s \sim I_0$. However, the generation frequency becomes saturated ($\Omega \to \Omega_{\max}$) with further intensity increase, when all of the donors are ionized and increasing I_s does not change the charge state of the crystal. The $\mathbf{q}$ vector is defined as a real one. Besides, it follows from Eq. (31) that the condition $Q_{||} < 0$ is necessary for observation of the AWLS. The latter restricts a class of materials where the optical autowaves can exist.

To amplify the backward wave, it is necessary that the condition $\exp[s_0 \ell] >> 1$ remain valid. In accordance with Eq. (32), this is possible only when $D < 0$, in compliance with a definite direction of the pump-beam propagation with respect to the polar axis *C*. The reason is that the coefficient $D \sim D_0 \chi_{13}$ changes its sign whenever the sample is rotated by 180 deg (i.e., under the change $z \to -z$). This corresponds to a bleaching regime, according to the classification given in Ref. [11].

Notice that the condition given by Eq. (31) defines only the magnitude of transverse part of the wave vector $\mathbf{q}$ of the grating, but not its direction. Therefore the pattern of the generation field should have axial symmetry with respect to the pump-beam centre.

Let us now consider the photoinduced bleaching regime ($D < 0$; $\exp[s_0 l] >> 1$). Using the above results, one can obtain the optical-field amplitude of the backward wave appearing on the front side of the sample ($z = 0$):

$$A_{-1}^*(x, y, 0, t) \approx -i\sqrt{I_0} \frac{\exp[s_0 \ell]}{\left(s_0 - iq_0^2/2k_0\right)} \int d\mathbf{q} \exp\left(-i\mathbf{q} \times \mathbf{r}_\perp\right) \times \tilde{W}(\mathbf{q}, s_0, t). \tag{33}$$

In Eq. (33), integration is performed over all of $\mathbf{q}$ vectors satisfying the condition $|\mathbf{q}| = q_0$ (see Eq. (31)). The temporal dependence of electrooptic modulation of the refractive index can be found from Eqs. (21), (28) and (30):

$$\tilde{W}(\mathbf{q}, s_0, t) = 2I_0 \frac{R_1(\mathbf{q})\alpha_2(q_0) - R_2(\mathbf{q})}{\alpha_1(q_0) - \alpha_2(q_0)} \exp\left(i\frac{\Omega}{2}t\right) \sin\left(\frac{\Omega}{2}t\right) [1 + \alpha_1(q)], \tag{34}$$

where the functions $R_{1,2}(\mathbf{q})$ and $\alpha_{1,2}(q_0)$ are specified by Eqs. (22). It is reasonable to assume that, for the samples with quasi-homogeneous distributions of photoactive impurities, the fluctuations $\delta n_d(\mathbf{r})$ manifest the following properties:

1 The second solution $\Omega_2 \approx 0$ is not associated with the AWLS effect.

$$\left\langle \tilde{R}_{1,2}(\mathbf{q}) \right\rangle = 0,\ \left\langle \tilde{R}_{1,2}(\mathbf{q}) \tilde{R}_{1,2}{}^{*}(\mathbf{q}') \right\rangle \sim \delta(\mathbf{q}-\vec{\mathbf{q}}') \left\langle \left| \tilde{R}_{1,2}(\mathbf{q}) \right|^2 \right\rangle . \tag{35}$$

Hereafter the angular brackets denote averaging over the random scattering sources.

The backward-wave field E_{-1} on the screen in the plane $z_S = -L$ may be found from Eq. (33) in the paraxial approximation, using the Fresnel–Kirchhoff formula [15]. In accordance with Eq. (35), statistical averaging of the parameter $\left|E_{-1}\right|^2$ is necessary to find the backward-wave intensity. When $\rho_0^2 << L/k_0$ and $L >> \ell$, the angular dependence of the backward AWLS indicatrix is described by the relation

$$J_{-1}(\theta,t) \approx \left(1-\cos(\Omega t)\right) \frac{\exp\left[-\Delta^2 \left(\theta-\theta_0\right)^2 / 2\right]}{1+\pi\Delta^2\theta_0\theta} \quad (0<\theta<<1), \tag{36}$$

where $J_{-1}(\theta,t) = \left\langle I_{-1}(\theta,t) \right\rangle \Big/ I_0 R_0^2$, $\theta_0 = q_0/k_0 << 1$ and $\Delta = k_0\rho_0$. One can see that the backward scattering is periodic in time (the frequency Ω) and has a conical spatial structure (the central angle θ_0).

4. Comparison with the experiment

Now let us compare the results of our theory and AWLS experiments. We remind that the samples of $LiNbO_3$ with the Fe concentrations (0.02÷0.07) weight % were observed in our study, and the optimal condition for the AWLS effect was 0.03 weight %. The maximum of the scattering cone corresponded to the angle $\theta_{\max} \approx \theta_0$. It is seen from Eqs. (14) and (31) that $q_0 \sim \left[\left|Q\right|_{\|}\right]^{1/2} \sim \left(n_d - n_{ds}^{+}\right)^{1/2}$. Bearing in mind only the generation-angle dependence on the concentration and supposing for rough estimation that $n_{ds}^{+} \approx n_a$, one finds

$$\theta_0 \approx \theta_f \left(n_d - n_a\right)^{1/2}, \tag{37}$$

where θ_f is a parameter of the theory. It is worth noticing that the photoactive-impurity concentration n_d represents one of the control parameters. In particular, the autowaves disappear at $n_d < n_a$.

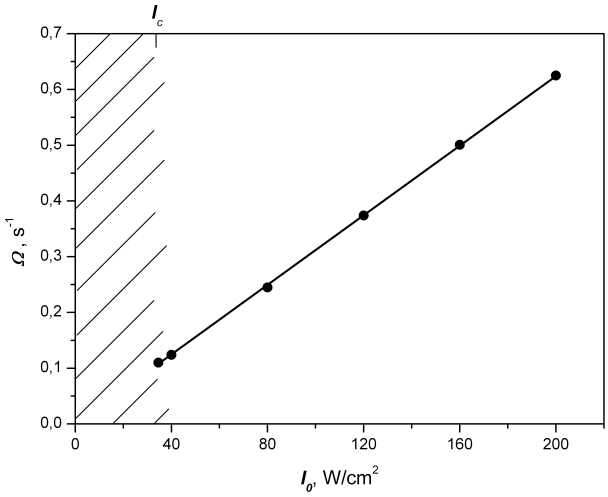

Fig. 3. Dependence of autowave frequency Ω on the pump intensity I_0. Solid curve corresponds to theoretical calculations and dots to experimental data (n_d = 0.03 weight %, λ = 0.44 μm and ℓ = 0.3 cm – see the text). The intensity region of the chaotic mode is shaded

The theoretical and experimental dependences of the autowave frequency Ω on the pump-wave intensity I_0 are represented in Fig. 3. In compliance with the experimental data, we have a linear dependence for sufficiently high pump intensities ($\gamma_p I_0 >> \gamma_T$):

$$\Omega(I_0) \cong C_f I_0 , \tag{38}$$

where C_f is proportional to the constant of photoconductivity. The pump-intensity threshold may be evaluated from the condition $s_0 \ell = 1$. Then the threshold intensity (see Eq. (32)) reads as

$$I_C \cong -\frac{1}{D\ell} \quad (D < 0) . \tag{39}$$

One can see that the pump intensity is also a control parameter. Moreover, the AWLS becomes possible only under the condition $I_0 > I_C$.

The spatial and temporal characteristics of periodic optical autowaves calculated theoretically above the threshold are in good agreement with the experimental data obtained for the $LiNbO_3$: Fe crystals. It should be stressed that the chaotic mode (i.e., pulsations of irregular spots) needs no competition of the transmitting and reflecting gratings and so can be reached below the threshold. This has been successfully demonstrated in Refs. [16, 17].

Basing on the theory and experiments reported in the present work, one can draw the following conclusions:

(1) To describe the effect of optical autowave generation, both the longitudinal and transverse photovoltaic/diffusive currents should be taken into account. Under the conditions discussed above, the transverse currents destroy a stationary charge redistribution created by the longitudinal currents, resulting in the appearance of cyclic (in time) charge transfer.

(2) The autowave light scattering represents a threshold effect: periodic in time, conically shaped pattern of radiation appears in the photorefractive crystals when the control parameters such as the pump intensity and the photoactive impurity concentration exceed the appropriate critical values.

Acknowledgement

The authors are grateful to A. Morozovska for her cooperation and aid in the preparation of this article to publication.

References

1. Lemeshko V V and Obukhovsky V V, 1985. Autowaves of photoinduced light scattering. Pisma Zhurn. Techn. Fiz. **11**: 573–574.
2. Liu Si-Min, Zhang Guang-Yin, Wang Jin-Long, Ma Xiao-Yan and Fu Yuan-Fen, 1989. Quasi-periodic oscillations in photoinduced conical light scattering from $LiNbO_3$:Fe crystals. Opt. Commun. **70**: 185–189.
3. Lemeshko V V, Obukhovsky V V and Stoyanov A V, 1992. Autowave origin under optical excitation of lithium niobate. Izv. RAN, Ser. Fiz. **56**: 7–14.
4. Furman A S, 1987. Spontaneous growth of trap charge exchange waves in crystals without inversion center under homogeneous illumination. Fiz. Tverd. Tela. **29**: 1076–1085.
5. Safiman M, Zozulya A and Anderson D Z, 1994. Transverse instability of energy-exchanging counterpropagating waves in photorefractive media. J. Opt. Soc. Amer. B. **11**: 1409–1417.
6. Leonardy J, Kaiser F, Belic M and Hess O, 1996. Running transverse waves in optical phase

conjugation. Phys. Rev. A. **53**: 4519–4527.
7. Sandfuchs O, Leonardy J, Kaiser F and Belic M, 1997. Transverse instabilities in photorefractive counterpropagating two-wave mixing. Opt. Lett. **22**: 498–500.
8. Haken H, Synergetics. Berlin–Heidelberg–New York: Springer (1978).
9. Morozovskaya A N and Obukhovskii V V, 2000. Autowave instability in refractive crystals. Opt. Spectr. **88**: 225–231.
10. Morozovskaya A N and Obukhovskii V V, 2005. Optical autowaves in photorefractive ferroelectric crystals. Opt. Spectr. **98**: 247–256.
11. Kukhtarev N V, Markov V B, Odulov S G, Soskin M M and Vinetskii V L, 1978. Holographic storage in electrooptic crystals. Ferroelectrics. **22**: 949–964.
12. Morozovska A N and Eliseev E A, 2004. Modeling of dielectric hysteresis loops in ferroelectric semiconductors with charged defects. J. Phys.: Condens. Matter. **16**: 8937–8956.
13. Morozovska A N, Eliseev E A, Svechnikov G S and Kalinin S V, 2011. Nanoscale electromechanics of paraelectric materials with mobile charges: Size effects and nonlinearity of electromechanical response of $SrTiO_3$ films. Phys. Rev. B. **84**: 045402.
14. Yariv A, Quantum electronics. Wiley (1989).
15. Born M and Wolf E, Principles of optics. Cambridge: Cambridge University Press (2002).
16. Shamonina E, Sturman B, Odoulov S and Ringhofer K, 1996. Investigation of stochastic photorefractive backscattering. J. Opt. Soc. Amer. B. **13**: 2242–2251.
17. Odoulov S, Sturman B, Shamonina E and Ringhofer K, 1996. Stochastic photorefractive backscattering from $LiNbO_3$ crystals. Opt. Lett. **21**: 854–856.

Obukhovsky V. and Lemeshko V. 2014. Optical chaos and oscillations in photorefractive $LiNbO_3$:Fe. Ukr.J.Phys.Opt. **15**: 68-78.

Анотація. *Автохвилі розсіяння з'являються при збудженні нелінійних кристалів* $LiNbO_3:Fe$ *сфокусованим лазерним випромінюванням і мають вигляд рухомих світлових кільцевих структур. Періодичну поведінку генерації кілець можна пов'язувати з конкуренцією ґраток показників заломлення двох типів – відбивного і пропускного. Якщо значення контрольних параметрів (інтенсивності нагнітання та концентрації домішок) нижчі за порогові, то виникає хаотичний режим розсіяння автохвиль.*